Available online at www.sciencedirect.com
SCIENCE DIRECT®
Earth and Planetary Science Letters 244 (2006) 683–694
EPSL
www.elsevier.com/locate/epsl

P–V–T relationships and mineral equilibria in inclusions in minerals

Michel Guiraud [a], Roger Powell [b,*]

[a] *USM 201, FRE CNRS 2456, Muséum National d'Histoire Naturelle, 61 rue Buffon, 75005, Paris, France*
[b] *School of Earth Sciences, University of Melbourne, Victoria 3010, Australia*

Received 9 May 2005; received in revised form 1 February 2006; accepted 14 February 2006
Available online 29 March 2006
Editor: G.D. Price

Abstract

When a mineral is included in another, the pressure on the two is the same. As pressure and temperature then change, the pressure on the inclusion is likely to become increasingly different to the pressure on its host as a consequence of the two minerals having different equations of state (i.e. pressure–volume–temperature *P–V–T* relationships). Under some limiting assumptions, including that the host behaves elastically, it is simple to calculate the under- or overpressure experienced by an inclusion along the *PT* path the host follows. By focussing diagrammatically on *V*, the natural variable, rather than the normally used conjugate variable, *P*, we represent the consequences of inclusion for arbitrary *PT* paths, giving the under- or overpressure as well as the equilibrium reaction progress if reaction in the inclusion is involved.

Keywords: mineral inclusions; *P–V–T* relations; coesite; diamond

1. Introduction

It is commonplace to use what is preserved as inclusions in a mineral to infer aspects of a rock's geological history, the idea being that the host mineral to the inclusions provides an inert container allowing minerals that have since reacted out of the matrix to nevertheless be preserved in the host mineral. This may or may not be a naïve interpretation of what the inclusion represents, given that, for example, the inclusion may have reacted with its host or exchanged elements with it subsequent to inclusion. Nevertheless such inclusions may provide the only evidence, however encoded, of the mineral assemblage in a rock when the host was growing. For example the existence of coesite or diamond inclusions in zircon and garnet has been used to suggest an ultrahigh pressure (uhp) history for rocks that otherwise show little or no evidence of such a history.

When the "inert container" analogy is appropriate, for example considering coesite or diamond inclusions in garnet, another aspect of inclusion can be considered: the pressure experienced by an inclusion departs from that acting on its host following inclusion, as a consequence of the different equations of state of the inclusion and host. At the time of being included, the inclusion is at the same pressure as the host, but if, for example, as *PT* changes the volume in the host which the inclusion initially occupied changes insufficiently to accomodate the change in volume of the inclusion, the pressure experienced by the inclusion will rise above that acting on the host. This effect is well known: in a linear elastic theory context such a situation has made it

* Corresponding author. Fax: +61 3 8344 7761.
E-mail address: powell@unimelb.edu.au (R. Powell).

0012-821X/$ - see front matter © 2006 Elsevier B.V. All rights reserved.
doi:10.1016/j.epsl.2006.02.021

into textbooks, e.g. [1]. Considerations based on this theory have been used in the geological literature since the 1960s, for example, in order to estimate pressure of equilibration from experimental measurements relating to dilatometry [2,3]. This experimental approach has been applied successfully to the garnet–quartz association in amphibolite facies pelitic rocks [4,5].

Renewed interest in the internal pressure on inclusions has been sparked by the discovery that, for example, coesite inclusions in garnet and zircon in ultrahigh pressure (uhp) rocks are at elevated pressures in the laboratory at the present day. This has been shown using laser Raman microspectrometry applied to inclusions that do not intersect the surface of the host and so may still be pressurised. Characteristic shifts in the Raman spectra reflect a preserved internal overpressure which can be used to estimate pressure of entrapment, e.g. [6,22,25]. However, wherever elastic theory has been used to decipher *PT* paths, e.g. [7], there has not been devised a useful diagrammatic representation of inclusion-host *P–V–T* relationships. Where diagrams have been involved at all, they have been *PT* ones, e.g. [8], with the path followed by an inclusion shown as separate from the one of the host, as in Fig. 1b. The inclusion's path—effectively a buffering path, a path buffered by the constraining effect of the host on the inclusion—cannot be deduced without considering the maths relating the relative volumes of inclusion and host.

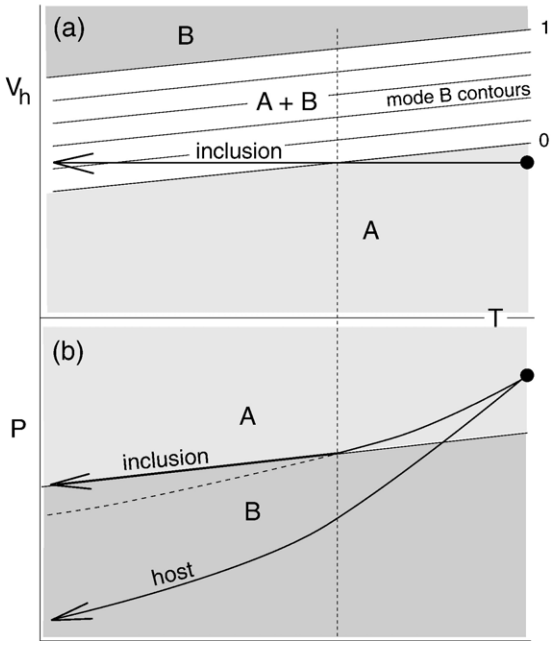

Fig. 1. (a) *V–T* and the equivalent *P–T* diagram, (b), showing the equivalence in terms of inclusion and host phase relationships and *PT* paths.

Thermodynamic variables occur in conjugate pairs involving corresponding intensive and extensive variables, only one of which can be used in a thermodynamic description of a system, e.g. [9]. In the current context, the conjugate pair of variables of interest is the intensive variable pressure, *P*, and the extensive variable volume, *V*. Of the intensive and extensive variables, the "natural" variable is the intensive one if the system being considered is at superimposed value of the intensive variable. This is commonly assumed to approximate the situation applying to many rocks during metamorphism, at least on an appropriate timescale, with *V* changes accomodated by deformation allowing *P* to be considered to be superimposed. This approximation is inappropriate in considering an inclusion unless the host mineral itself is able to deform. In the absence of such deformation, volume is the natural variable, thermodynamically, as well as rather obviously via the volume constraint created by the hole occupied by the inclusion in the host mineral. This is well known to those dealing with the interpretation of fluid inclusions, e.g. [10]. In fluid inclusion theory, *T−V*, or rather, *T−density* diagrams are the primary source of information. However, as acknowledged by Roedder ([10] p.230), such diagrams look unusual to most geologists and therefore *P−T* diagrams contoured for isochores have been the preferred way of representing the information. Yet *V* (or density) is the natural variable and we pursue in this paper the aim of showing the usefulness of using *V* as an axis on diagrams considering inclusions in minerals, as indeed advocated by Zhang [11].

Represented in Fig. 1 is an idealised situation in which a fixed size hole in the host, represented by V_h in Fig. 1a, is filled with an inclusion of a higher pressure phase A. It is assumed that A expands as *PT* decreases. As represented in Fig. 1b, A has a lower pressure form, B. In such a constant volume situation, the horizontal arrow in Fig. 1a represents the evolution of the inclusion, with a small conversion of A to B occurring once the two-phase field in Fig. 1a is intersected. As shown in Fig. 1b, this simple *V–T* behaviour is reflected in the divergence of the inclusion *PT* path from that of its host, with eventual buffering of the inclusion path along the A=B univariant boundary. Note that this univariant, which is a line in *PT* is a field in *VT*.

Unfortunately, such an idealised situation cannot be applied to nature as the size of the hole occupied by the inclusion also varies with *PT*, and there is a feedback regarding the pressure experienced by the inclusion

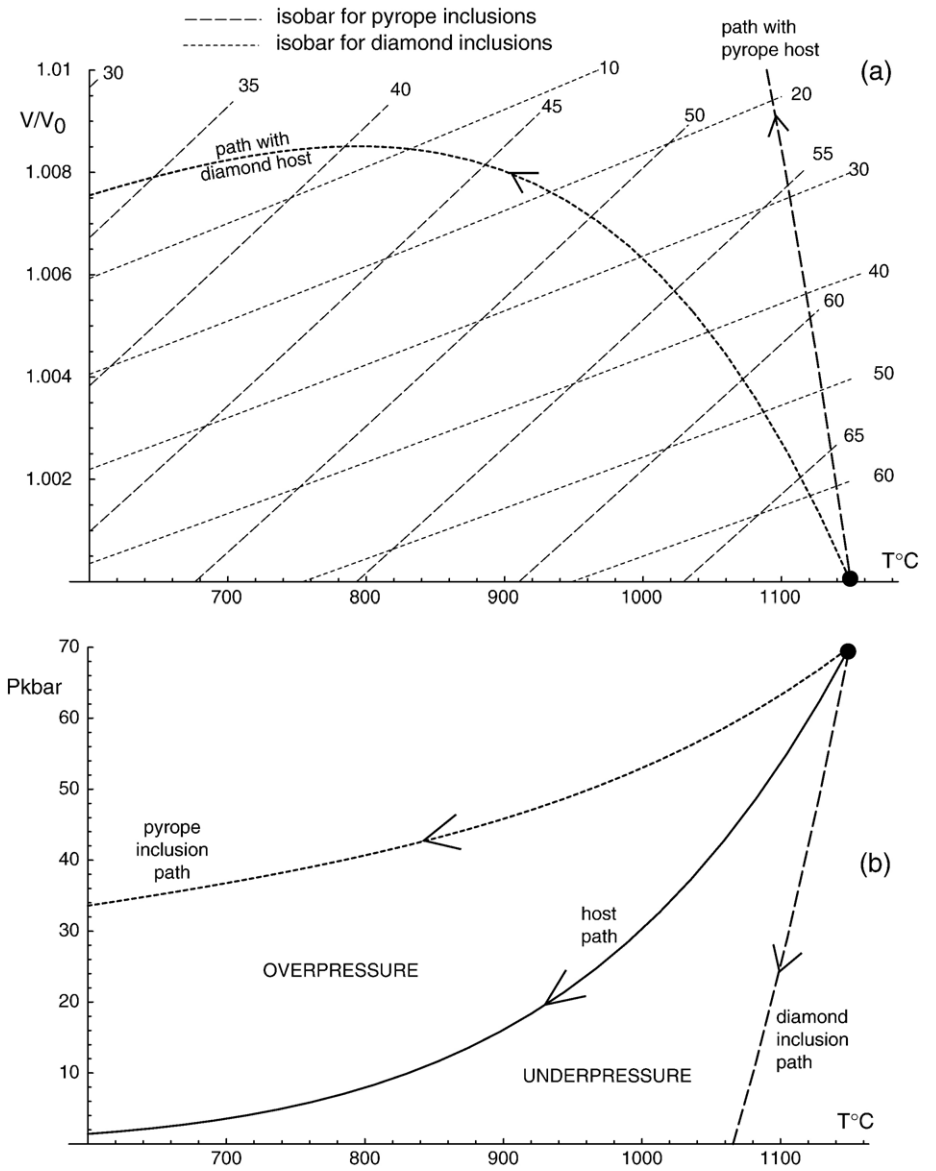

Fig. 2. (a) $\frac{V}{V_0}-T$ diagram for decompression and cooling from 70 kbar and 1150 °C for arbitrary *PT* paths. Shown on (a) are identical example *PT* paths for pyrope in diamond and diamond in pyrope, and in (b) the equivalent path relationships in *P*–*T*. With respect to the host *PT* path, diamond as inclusion involves underpressure; pyrope overpressure. These diagrams ignore the effect of the shear modulus of the host in the calculations.

provided by the elastic strain in the host adjacent to the inclusion. However, we have devised a powerful new way of representing the *P*–*V*–*T* relationships of inclusions based on the idea of *V*–*T* diagrams, and this is the focus of this paper.

2. *P*–*V*–*T* relationships

Using subscript i for inclusion, and h for host, and subscript 0 for the conditions at which inclusion takes place, then $(P_0, T_0)_i=(P_0, T_0)_h$. *PT* conditions in the host subsequent to inclusion, beyond the sphere of influence of inclusions and corresponding to the *PT* imposed on the rock as a whole, are denoted (*P*, *T*). Writing volume as an explicit function of *P* and *T*, *V* (*P*, *T*), the volume of the inclusion at (*P*, *T*) is $V_i(P_i, T)$. To determine P_i, the relative volume changes of the inclusion and the host are taken into account, moderated by the effect of the elastic strain of the host caused by the pressure difference, P_i–*P*. Following [2,3,7,12,13,11], assuming that linear elastic theory is appropriate, that the inclusion is small relative to the size of its host, and that the inclusion is

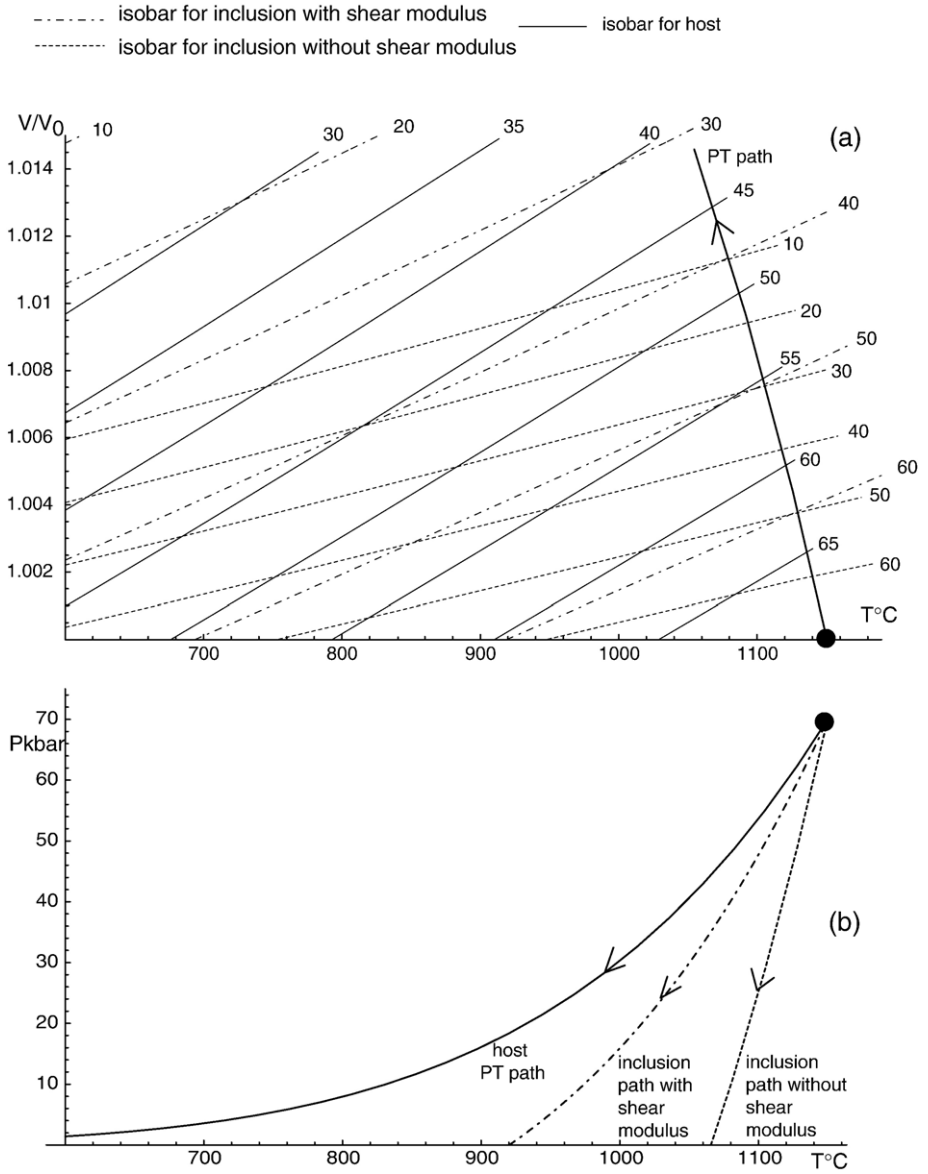

Fig. 3. (a) $\frac{V}{V_0}-T$ and (b) P–T diagrams, equivalent to the diamond in pyrope case in Fig. 2, showing the moderating effect of including the shear modulus of the host, pyrope.

sufficiently far away from other inclusions and from the edge of the host, P_i corresponding to (P, T) can be determined from:

$$\frac{V_h(P,T)}{V_h(P_0,T_0)}=\frac{V_i(P_i,T)}{V_i(P_0,T_0)}-\frac{3}{4G}(P_i-P) \quad (1)$$

in which G is the shear modulus of the host. All of the diagrams below are calculated via this controlling equation. The left hand side will be referred to as $\left(\frac{V}{V_0}\right)_h$, and the first term on the right hand side as $\left(\frac{V}{V_0}\right)_i$. Referring to both terms on the right hand side as the effective volume ratio for the inclusion, $\left(\frac{V}{V_0}\right)_i^{\text{eff}}$, then

$$\left(\frac{V}{V_0}\right)_i=\left(\frac{V}{V_0}\right)_h^{\text{eff}}$$

The new diagram introduced in this paper involves $\frac{V}{V_0}$ plotted against T, with $\left(\frac{V}{V_0}\right)_h$ representing the host, and $\left(\frac{V}{V_0}\right)_i^{\text{eff}}$ representing the inclusion, contoured for the P on the host and the P on the inclusion. For any arbitrary

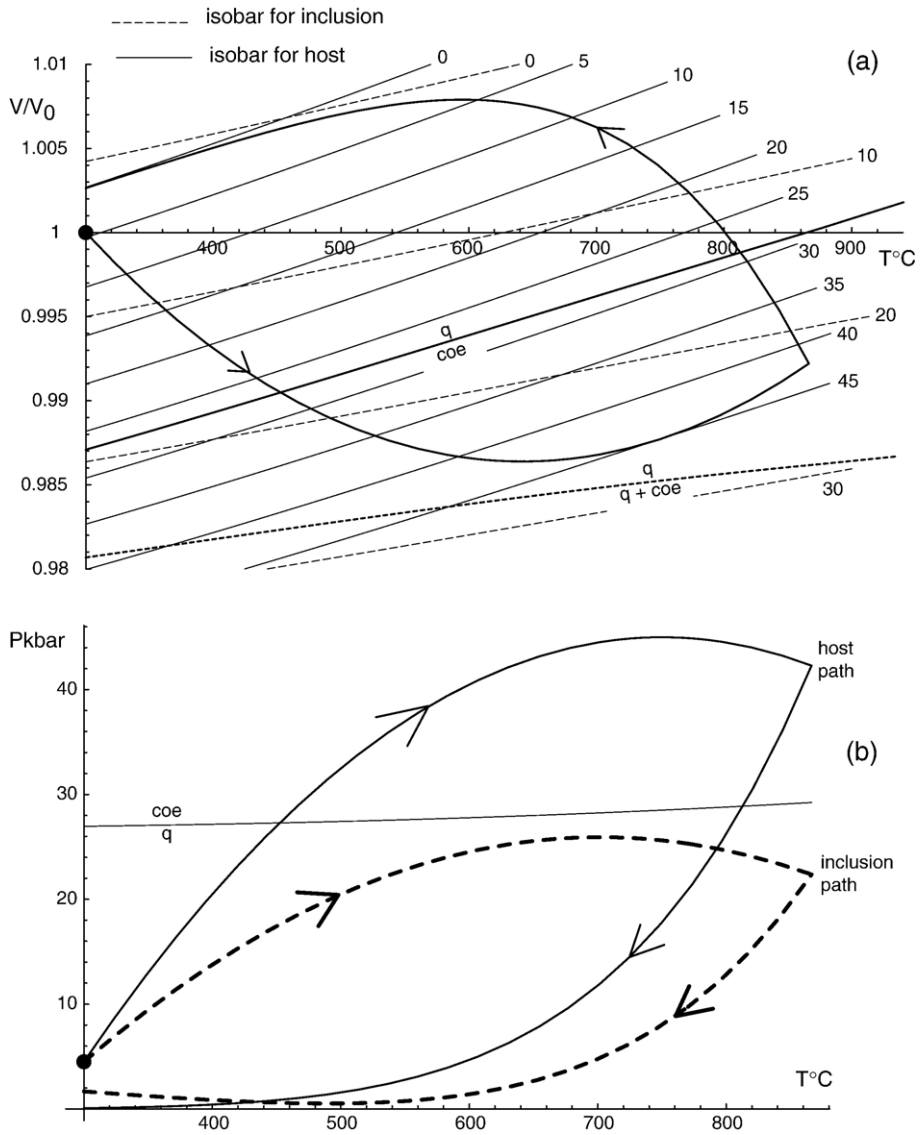

Fig. 4. (a) $\frac{V}{V_0}-T$ diagram for arbitrary *PT* paths from 3 kbar and 300 °C for quartz in garnet. The quartz=coesite reaction as would be seen by matrix quartz is shown, as well as the boundary of the quartz+coesite two-phase field that would be experienced by quartz inclusions. Shown on (a) is an example uhp *PT* path, and in (b) the equivalent path relationships in *P–T*. The inclusion path does not extend out of the quartz stability field.

PT path for the host from a specified starting point (P_0, T_0), the corresponding *PT* path followed by an inclusion is given. Such diagrams are presented and discussed for garnet included in diamond, diamond included in garnet, and quartz and coesite included in garnet. In the following it is assumed that thermodynamic equilibrium applies and that the minerals behave elastically. The data used for the volume calculations is from [14], with the shear moduli, $G_{\mathrm{diam}}=536$ GPa and $G_{\mathrm{py}}=97.3$ GPa.

3. $\frac{V}{V_0}-T$ diagrams

3.1. Ignoring the shear modulus

The simplest form of the diagram is where the shear modulus of the host is assumed infinite, so $\left(\frac{V}{V_0}\right)_{\mathrm{i}}^{\mathrm{eff}}=\left(\frac{V}{V_0}\right)_{\mathrm{i}}$, and no reaction in the inclusion takes place, Fig. 2. This figure, for pyrope-diamond, allows consideration of the *P–V–T* relationships of both pyrope inclusions in diamond and diamond inclusions in pyrope

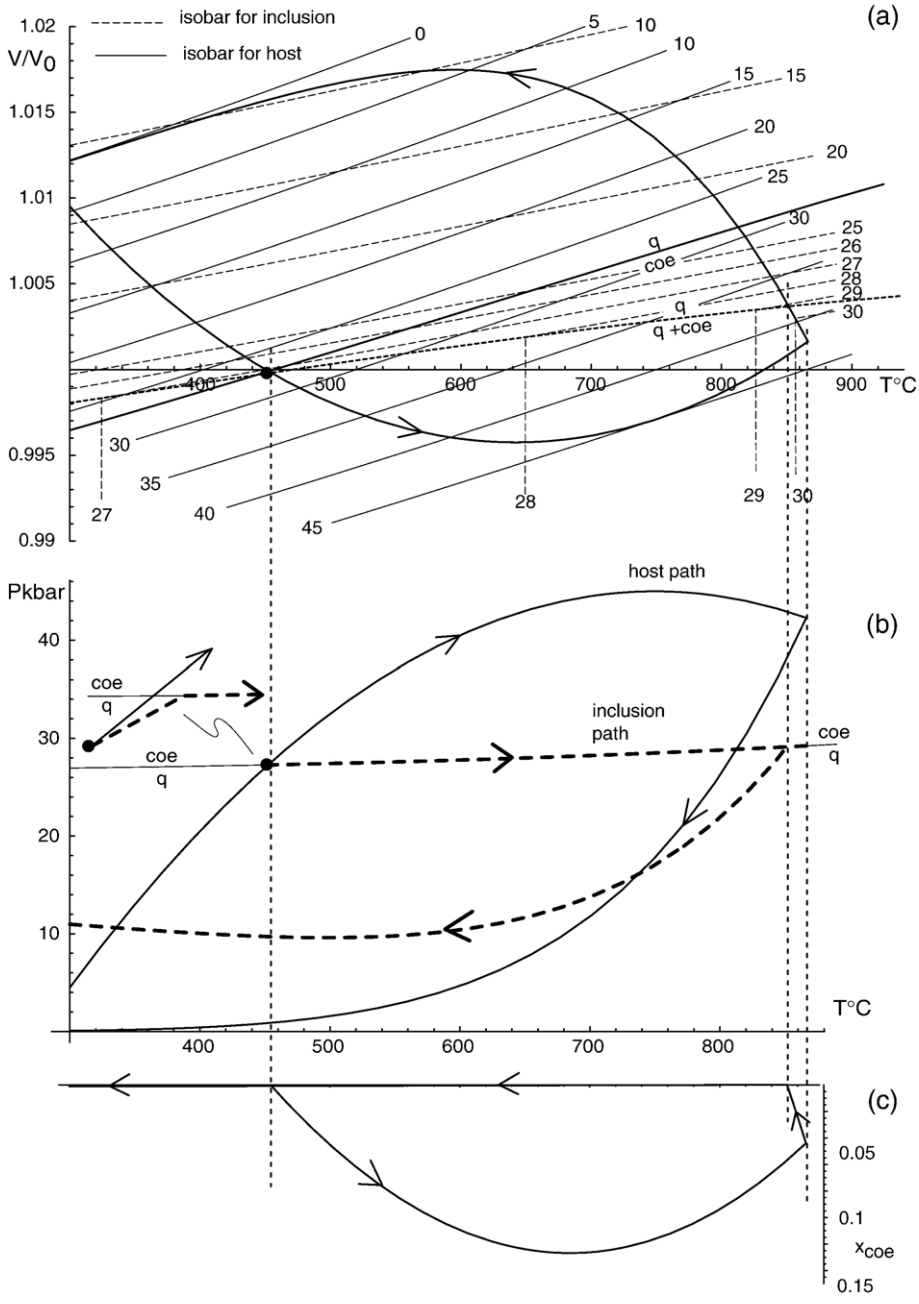

Fig. 5. (a) $\frac{V}{V_0}-T$ diagram for arbitrary *PT* paths for quartz in garnet from a starting (*PT*) point just inside the quartz stability field on the same example *PT* path used in Fig. 4. The inclusion path enters the quartz+coesite stability field in (a), and equivalently passes along the quartz=coesite reaction line in (b), but the inclusion reaches the Earth's surface as quartz. (c) $x_{coe}-T$ diagram showing the change in coesite fraction along the *PT* path.

during decompression and cooling from, in this case, 70 kbar and 1150 °C. Any host *PT* decompression and cooling path from this starting *PT* can be considered: the one used as an example is the solid line in Fig. 2b. Corresponding to this line are the $\left(\frac{V}{V_0}\right)-T$ inclusion paths in Fig. 2a: the heavy dashed line for pyrope as host, the light dashed line for diamond as host. To see the overpressure or underpressure involved with an inclusion path, the intersection of the path with the appropriate isobars is used, this information then being transferred to Fig. 2b as an inclusion *PT* path. For pyrope inclusions in diamond, the dashed pressure contours in Fig. 2a are used; for diamond inclusions in pyrope the dotted pressure contours. As can be seen,

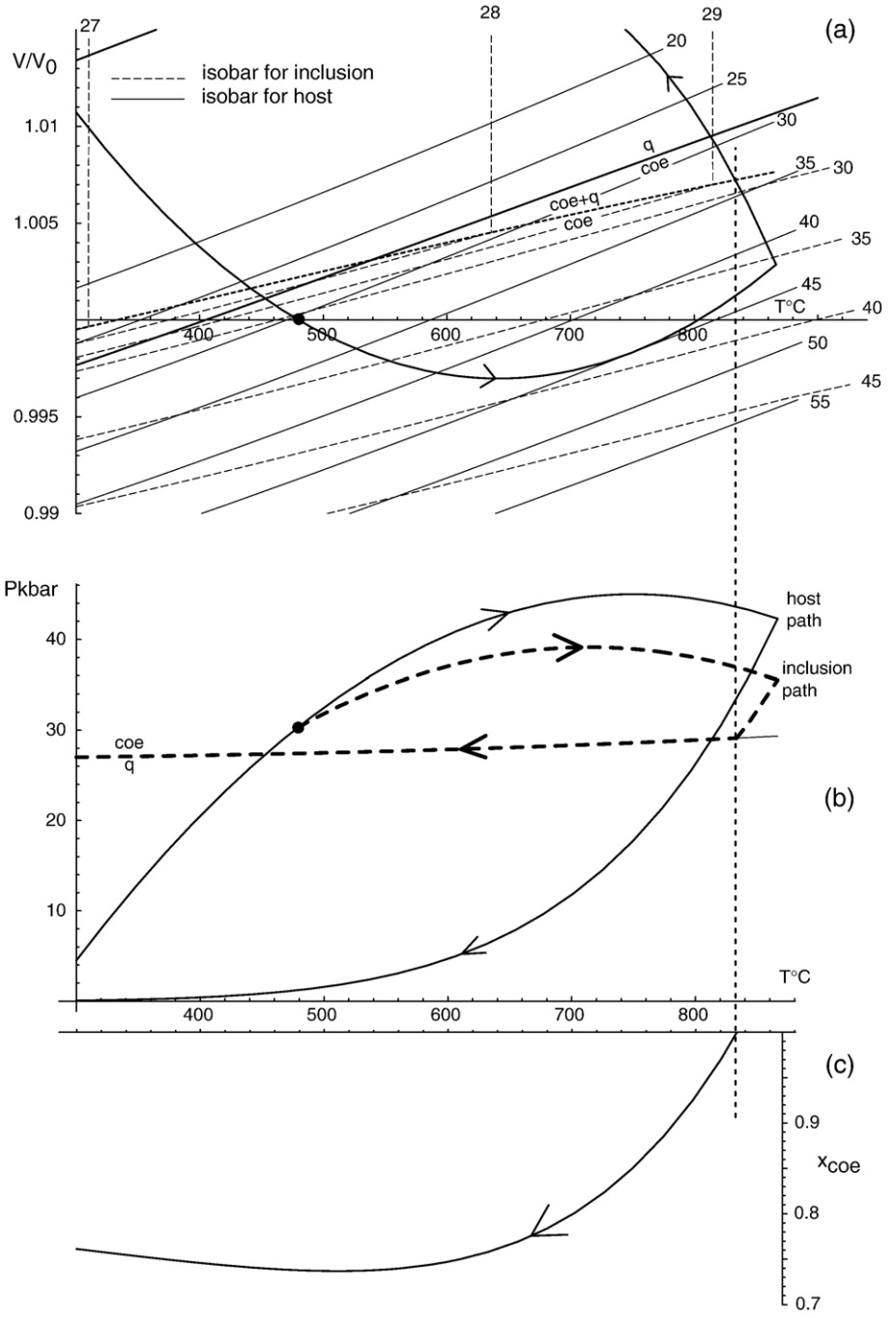

Fig. 6. (a) $\frac{V}{V_0}-T$ diagram for arbitrary *PT* paths for coesite in garnet from a starting (*PT*) point just across the quartz=coesite reaction line on the same example *PT* path used in Fig. 4. The inclusion path eventually enters the quartz+coesite stability field in (a), and equivalently passes along the quartz=coesite reaction line in (b); the inclusion reaches the Earth's surface with a significant proportion of the coesite having been transformed to quartz. (c) $x_{coe}-T$ diagram showing the change in coesite fraction along the *PT* path.

diamond inclusions are underpressured during decompression and cooling, whereas pyrope inclusions are overpressured, as a consequence of the relative *P–V–T* behaviour of the two phases.

When the shear modulus of the host is included in the calculation, there are two consequences. One is that the same diagram cannot be used for pyrope in diamond and diamond in pyrope because the shear

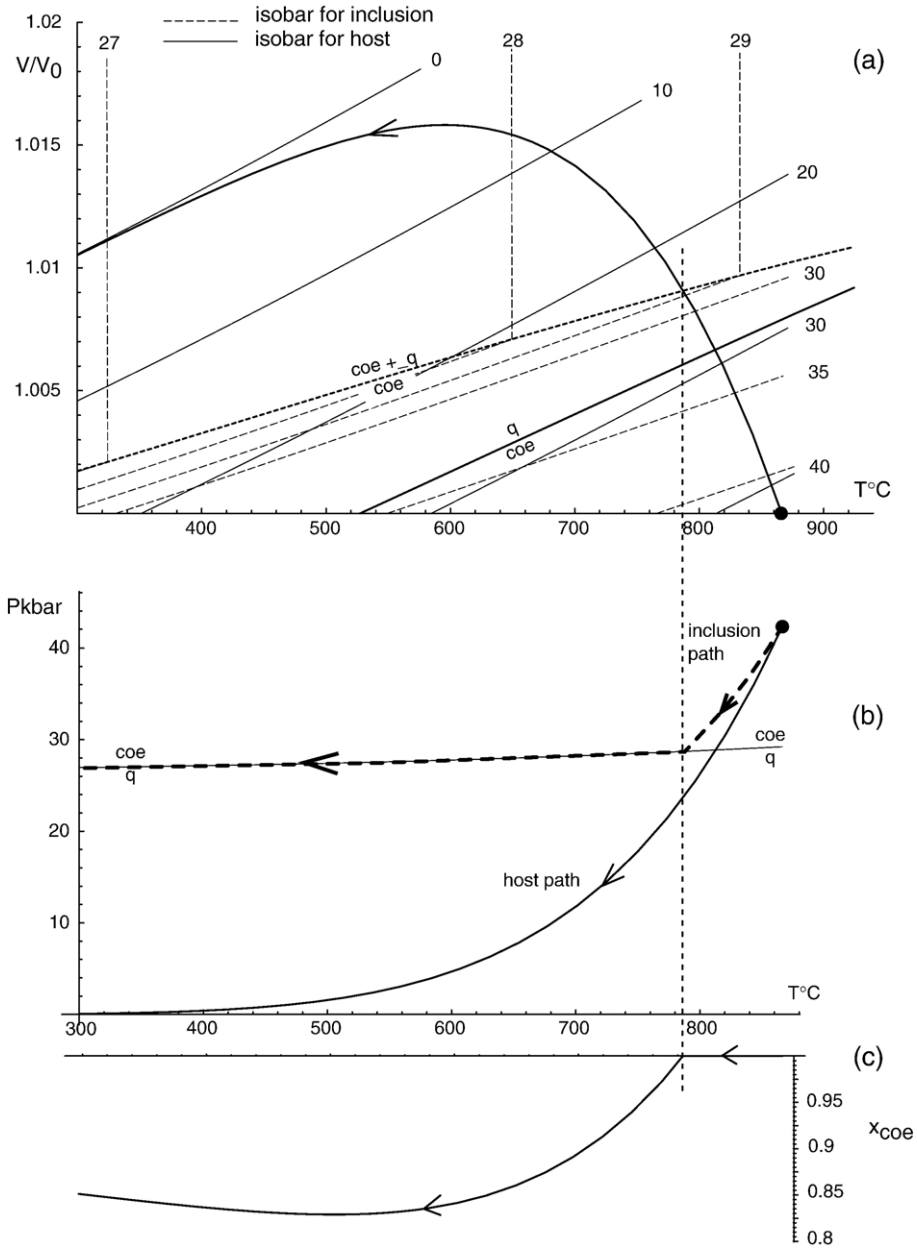

Fig. 7. (a) $\frac{V}{V_0}-T$ diagram for arbitrary *PT* paths for coesite in garnet from a starting (*PT*) point at peak *PT* conditions on the same example *PT* path used in Fig. 4. The inclusion path enters the quartz+coesite stability field in (a), and equivalently passes along the quartz=coesite reaction line in (b), but the inclusion reaches the Earth's surface mainly as coesite. (c) $x_{coe}-T$ diagram showing the change in coesite fraction along the *PT* path.

moduli of pyrope and diamond are different. The second is that the effect of including the shear modulus is to decrease the magnitude of over- or underpressure involved. This can be seen in Fig. 3 for diamond inclusions in pyrope. Comparing Figs. 2a and 3a, the pressure contours for diamond have contracted towards the path's starting point, meaning that underpressure of the inclusions is reduced, as shown in Fig. 3b. All the diagrams presented below were calculated including the shear modulus.

3.2. Quartz-coesite inclusions in pyrope

$\frac{V}{V_0}-T$ diagrams can also be used where reaction is involved, in this case using a simplified model of the spatial relationships in the inclusion such that both

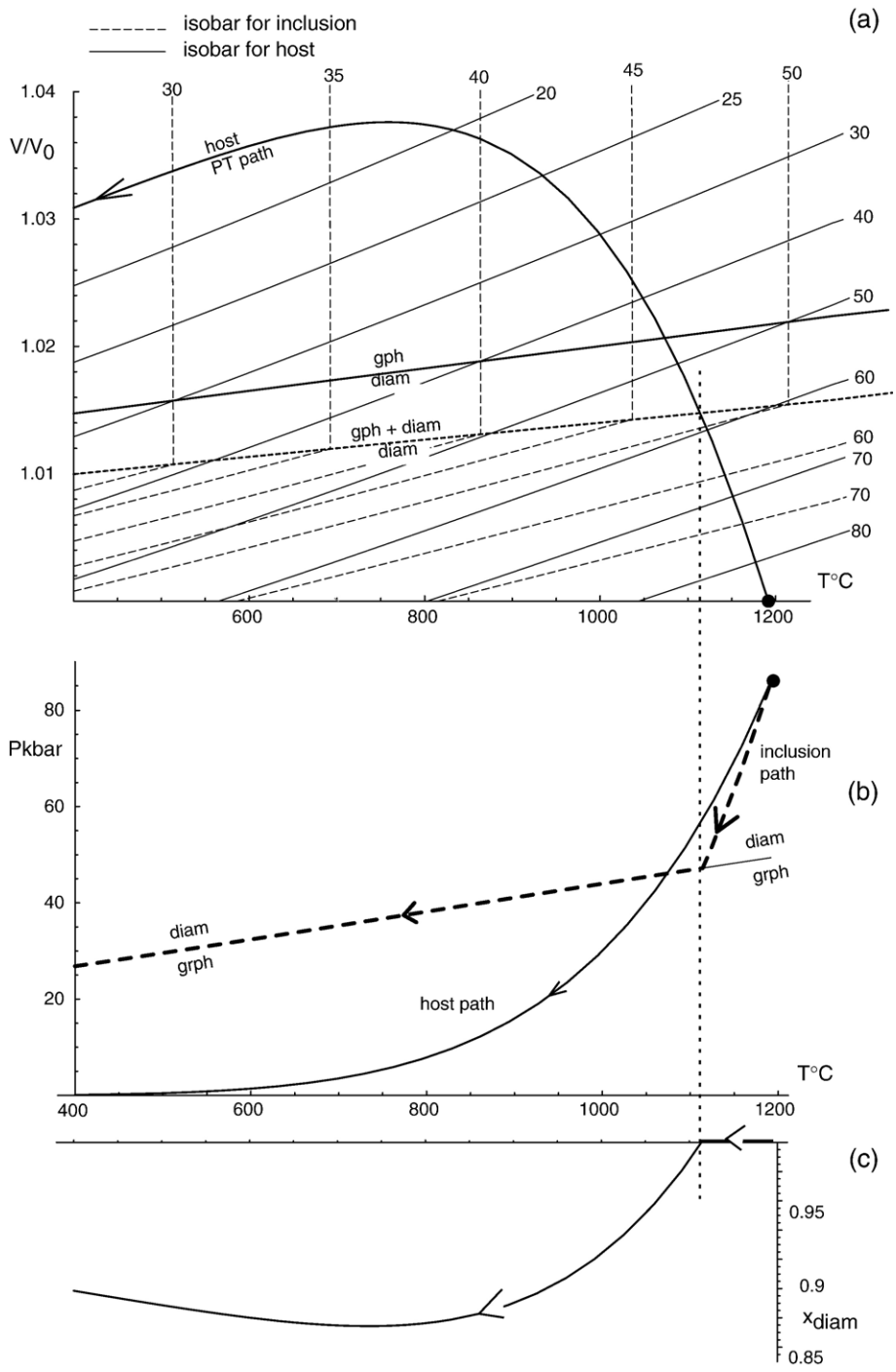

Fig. 8. (a) $\frac{V}{V_0}-T$ diagram for arbitrary decompression and cooling *PT* paths from 90 kbar and 1200 °C for diamond in pyrope. The inclusion path enters the diamond + graphite stability field in (a), and equivalently passes along the diamond = graphite reaction line in (b), but the inclusion reaches the Earth's surface mainly as diamond. (c) x_{diam}–T diagram showing the change in coesite fraction along the *PT* path.

product and reactant are at the inclusion pressure (c.f. [15]). Again the diagrams can be used to look at arbitrary host *PT* paths, and the corresponding inclusion *PT* paths. Where reaction commences in the inclusions can be shown, the subsequent modal evolution of the inclusion cannot be represented in a general way, by for

example contours, because the modes depend on the *T* where the reaction is intersected.

A key issue in considering the fate of inclusions is the *PT* conditions of inclusion along the *PT* path, and the next four diagrams address this for the inclusion of quartz or coesite in garnet. In Fig. 4, inclusion of quartz takes place at low *PT*, with the example host *PT* path shown extending to uhp conditions. The *PT* line marking the edge of the quartz+coesite field is shown (dotted line, Fig. 4a), along with the *PT* locus of the quartz=coesite reaction for the matrix of the rock (solid line, Fig. 4a). In this case, although the *PT* path extends well into the coesite stability field, the inclusion *PT* path remains within the quartz stability field reflecting the underpressure along the *PT* path (Fig. 4b). In contrast, as portrayed in Fig. 5, with inclusion of quartz taking place close to the limit of the quartz stability field, the inclusion *PT* path does enter the quartz+coesite stability field in Fig. 5a. However, as is shown in Fig. 5c, little coesite is produced for this path. The inclusion is buffered along the quartz=coesite univariant line in Fig. 5b, with the inclusion pressure contours in Fig. 5a therefore being vertical in the quartz+coesite field. The small amount of coesite produced is then reacted back to quartz as decompression and cooling gets under way. Reiterating a well-known result, e.g. [7,12], coesite inclusions in garnet cannot be made from originally included quartz.

If coesite is included in pyrope at immediately higher pressure from the *PT* of inclusion in Fig. 6, just into the coesite field, then the outcome is quite different for the inclusion, with coesite largely preserved, but with a significant amount of quartz being produced during buffering along the coesite=quartz reaction. If instead coesite is included at peak conditions, Fig. 7 can be used to consider the evolution of the inclusions for different paths during decompression and cooling, with the same example path shown in Fig. 7a, and the consequent inclusion path shown in Fig. 7b. This path is buffered along the coesite=quartz univariant line with a small proportion of quartz being formed, Fig. 7c. Thus such paths allow the majority of the coesite to be preserved, with the coesite overpressured at the Earth's surface.

The volume fraction of coesite in the inclusion depends on the *PT* path, and more precisely on the starting point along the *PT* path when coesite is included, and on the *PT* conditions where the coesite=quartz reaction is crossed. Calculations show there is a general trend: the higher the starting pressure, the larger volume fraction of coesite will remain at low *PT*, although this cannot be formulated for geobarometric purposes.

3.3. Diamond–graphite inclusions in pyrope

As shown in Fig. 2, diamond inclusions in pyrope, in contrast to coesite inclusions, become underpressured during cooling and decompression. From the indicated starting *PT*, all cooling and compression paths can be considered in Fig. 8a, including diamond–graphite reaction, with an example path shown. The inclusion path and the amount of conversion of diamond to graphite are shown on Fig. 8b and c. Once the diamond=graphite univariant line is intersected on Fig. 8b, or equivalently the diamond+graphite two-phase field entered on Fig. 8a, the inclusion is buffered by the reaction and the diamond remains overpressured to the Earth's surface.

4. Discussion

A general conclusion that can be drawn is that inclusions, at least ones that do not react with their host, tend to be preserved in the form that they were included, and this is a satisfactory result in the context of the occurrence of different polymorphs in different parts of host minerals. Thus quartz occurring as inclusions in the cores of garnet, but coesite in mantles, e.g. [8], and the same arrangement but in zircon, e.g. [19], can be understood in terms of the quartz inclusions having been enclosed in the quartz stability field, and the coesite inclusions in the coesite stability field. There are additionally definite predictions regarding the over-pressuring in different inclusions that arise from consideration of the above figures, considered further below.

Whether a mineral is included in a host mineral obviously depends on the petrological evolution of the rock, not only in mineral assemblage, but also in mineral modes. For garnet to include quartz then coesite involves the strong requirement that the mode of garnet is increasing in both the quartz and the coesite stability fields. This is open to prediction via the calculation of pseudosections, given the chemical composition of the part of the rock that the garnet is growing in [16]. Considering whiteschists, the pseudosection for the Parigi pyrope–coesite rock (Dora Maira) in Fig. 6 of [17] shows that for this low-Mn bulk composition, garnet does not grow til near-peak conditions at pressures above 30 kbar, well within the coesite stability field. It is not surprising therefore that the pyrope contains coesite inclusions [18]. In contrast, more manganiferous whiteschists, e.g. [8], will start to grow garnet much earlier in the mineral assemblage evolution of the rock, as a consequence of manganese stabilising

garnet, and in that case garnet started to grow in the quartz stability field. The more manganese-rich cores of the garnet contain quartz inclusions, whereas the mantles contain coesite inclusions [8], the latter correspond to continuing near-peak garnet growth as in the Dora Maira whiteschist.

The use of Raman methods has revolutionised consideration of the overpressures developed in inclusions by allowing present-day overpressures to be deduced via the experimentally determined shift of peaks in Raman spectra. With a simple elastic model, and in the absence of disruption of the inclusion by strain, including overpressure-induced strain, and strain during sample preparation, the above figures predict the Raman shifts. Thus coesite inclusions in both diamond and garnet should be overpressured at around 25 kbar, regardless of the initial *PT* of inclusion, and regardless of the proportion of the lower pressure form developed. Overpressures in quartz inclusions are predicted to have Raman shifts corresponding to 10 kbar or less. Polycrystalline quartz inclusions, e.g. [26], are unlikely to be recrystallised coesite inclusions if they are overpressured, but may have just intersected the quartz=coesite reaction, so representing inclusion at relatively high pressure but outside the coesite stability field.

The simple elastic model used here results in only a small proportion of quartz developed in a coesite inclusion in garnet at the end of the *PT* evolution, e.g. Figs. 6 and 7. Assuming a spherical inclusion, the diameter of coesite grain represents at least about 95% of the diameter of inclusion, but in many natural samples the coesite/quartz ratio is much smaller (e.g. [26]). The amount of reaction beyond that predicted with the *V–T* logic above is a consequence of the (partial) release of the overpressure causing an effective increase of volume of the inclusion. Such an increase of volume is most likely reflected in the (radial) cracking of the host mineral; the preservation of any coesite may then be kinetically controlled. It is not clear whether polycrystalline quartz inclusions with radial cracking around them can be due to failure of overpressured quartz inclusions whose host did not in fact enter the coesite field.

A consequence of taking a *V–T* view of the history of inclusions in minerals is that it is possible to have a clearer idea of what is the cause and effect in reaction in inclusions, the development of overpressure and the associated development of deformation features (for example radial cracking around inclusions). For example, saying overpressures are induced by the coesite–quartz transition in zircon or garnet is not correct (e.g. [24]). The overpressuring is due to the differential expansion of the inclusion and host. Further, the *V–T* view allows it to be seen clearly that the *PT* of inclusion plays a fundamental role in controlling the subsequent evolution of inclusions. Beyond reflecting the *PT* stability field in which inclusion takes place, there is little direct thermobarometric information in inclusions (c.f. [27]).

Acknowledgements

We would like to thank the reviewers for their comments, and Tim Holland and Richard White for discussions.

References

[1] R.V. Southwell, An Introduction to the Theory of Elasticity for Engineers and Physicists, Oxford University Press, Oxford, 1941, 509 pp.
[2] J.L. Rosenfeld, A.B. Chase, Pressure and temperature of crystallization from elastic effects around solid inclusions in minerals? Am. J. Sci. 261 (1961) 519–554.
[3] J.L. Rosenfeld, Stress effects around quartz inclusions in almandine and the piezothermometry of coexisting aluminium silicates, Am. J. Sci. 267 (1969) 317–351.
[4] H.G. Adams, L.H. Cohen, J.L. Rosenfeld, Solid inclusion piezothermometry: I. Comparison dilatometry, Am. Mineral. 60 (1975) 574–583.
[5] H.G. Adams, L.H. Cohen, J.L. Rosenfeld, Solid inclusion piezothermometry: II. Geometric basis, calibration for the association quartz–garnet, and application to some pelitic schists, Am. Mineral. 60 (1975) 584–598.
[6] C.D. Parkinson, I. Katayama, Present-day ultrahigh-pressure conditions of coesite inclusions in zircon and garnet: evidence from laser Raman microspectroscopy, Geology 27 (1999) 979–982.
[7] P. Gillet, J. Ingrin, C. Chopin, Coesite in subducted continental crust: *P–T* history, Earth Planet. Sci. Lett. 70 (1984) 426–436.
[8] C.D. Parkinson, Coesite inclusions and prograde compositional zonation of garnet in whiteschist of the HP-UHPM Kokchetav massif, Kazakhstan: a record of progressive UHP metamorphism, Lithos 52 (2000) 215–233.
[9] R. Powell, M. Guiraud, R.W. White, Conjugate thermodynamic variables and equilibrium phase diagrams, Can. Mineral. 43 (2005) 21–33.
[10] E. Roedder, Fluid inclusions, Reviews in Mineralogy, vol. 12, Mineralogical Society of America, 1984, p. 646.
[11] Y. Zhang, Mechanical and phase equilibria in inclusion-host systems, Earth Planet. Sci. Lett. 157 (1998) 209–222.
[12] I. van der Mohlen, H.L.M. van Roermund, The pressure path of solid inclusions in minerals: the retention of coesite inclusions during uplift, Lithos 19 (1986) 317–324.
[13] S. Tait, Selective preservation of melt inclusions in igneous phenocrysts, Am. Mineral. 77 (1992) 146–155.
[14] T.J.B. Holland, R. Powell, An internally-consistent thermodynamic dataset for phases of petrological interest, J. Metamorph. Geol. 16 (1998) 309–344.

[15] T. Nishiyama, Kinetic modelling of the coesite–quartz transition, The Island Arc, vol. 7, 1998, pp. 70–75.
[16] R. Powell, T.J.B. Holland, B. Worley, Calculating phase diagrams involving solid solutions via non-linear equations, with examples using THERMOCALC, J. Metamorph. Geol. 16 (1998) 577–588.
[17] R. Coggon, T.J.B. Holland, Mixing properties of phengitic micas and revised garnet–phengite thermobarometers, J. Metamorph. Geol. 20 (2002) 683–696.
[18] C. Chopin, Coesite and pure pyrope in high-grade blueschists in the Western Alps: a first record and some consequences, Contrib. Mineral. Petrol. 86 (1984) 107–118.
[19] F. Lui, Z. Xu, J.G. Liou, I. Katayama, H. Masago, S. Maruyama, J. Yang, Ultrahigh pressure mineral inclusions in zircons from gneissic core samples of the Chinese Continental Scientific Drilling Site in eastern China, Eur. J. Mineral. 14 (2002) 499–512.
[22] E.S. Izraeli, J.W. Harris, O. Navon, Raman barometry of diamond formation, Earth. Planet. Sci. Lett. 173 (1999) 351–360.
[24] K. Ye, J.-B. Liou, B. Cong, S. Maruyama, Overpressures induced by coesite–quartz transition in zircon, Am. Mineral. 86 (2001) 1151–1155.
[25] N.V. Sobolev, B.A. Fursenko, S.V. Goryainov, J. Shu, R.J. Hemley, H. Mao, F.R. Boyd, Fossilized high pressure from the Earth's deep interior: the coesite-in-diamond barometer, Proc. Natl. Acad. Sci. U. S. A. 22 (2000) 11875–11879.
[26] A. Wain, D. Waters, A. Jephcoat, H. Olijynk, The high-pressure to ultrahigh-pressure eclogite transition in the Western Gneiss Region, Norway, Eur. J. Mineral. 12 (2000) 667–687.
[27] L.M. Barron, A linear model and topology for the host-inclusion mineral system involving diamond, Can. Mineral. 43 (2005) 203–224.